Volume 15 | Number 30 | 14 August 2019 | Pages 6029–6248

Soft Matter

rsc.li/soft-matter-journal

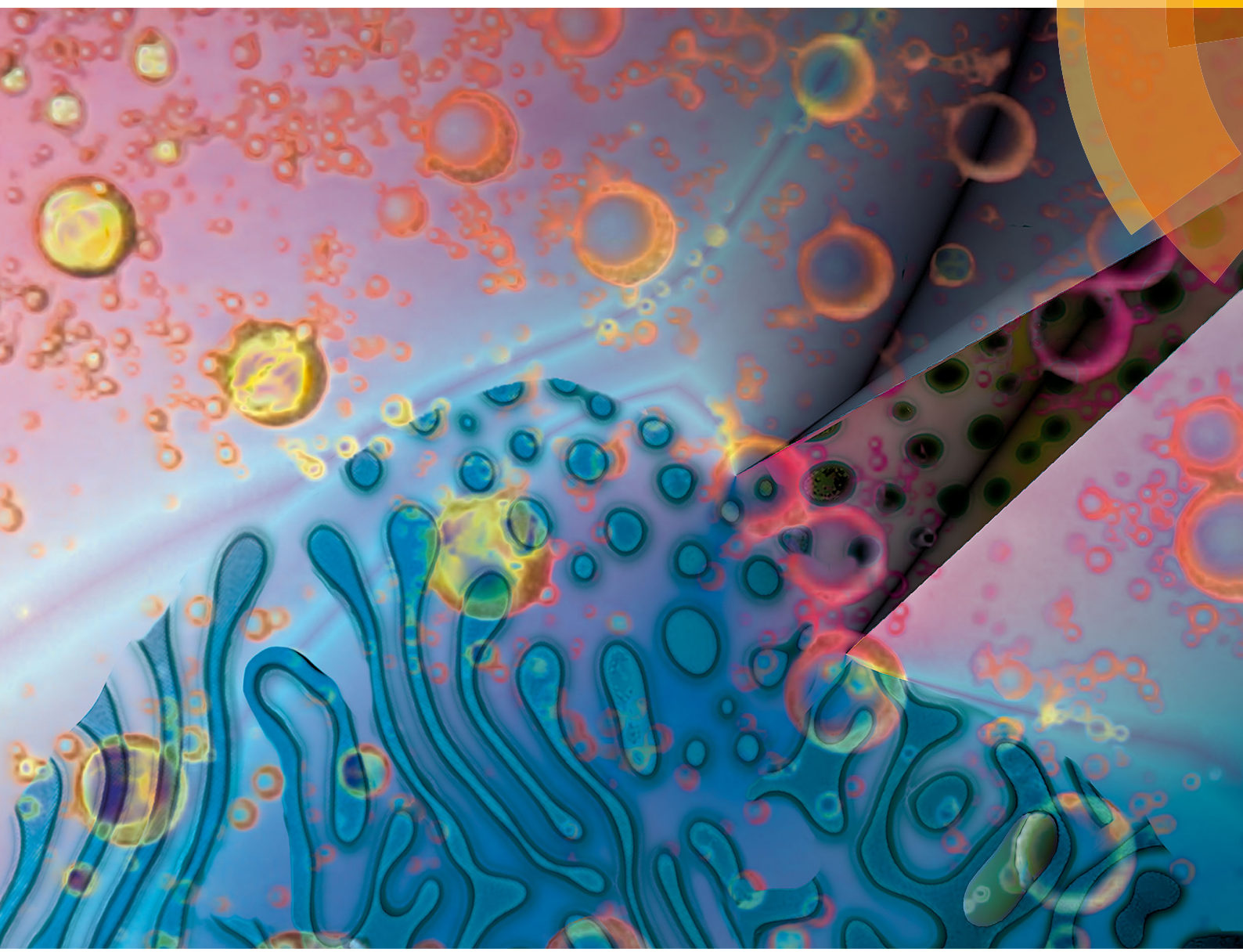

ISSN 1744-6848

ROYAL SOCIETY OF CHEMISTRY | Celebrating IYPT 2019

PAPER
Takeaki Araki, Jan P. F. Lagerwall *et al.*
Isotropic–isotropic phase separation and spinodal decomposition in liquid crystal–solvent mixtures

Soft Matter

PAPER

View Article Online
View Journal | View Issue

Cite this: *Soft Matter*, 2019, **15**, 6044

Isotropic–isotropic phase separation and spinodal decomposition in liquid crystal–solvent mixtures†

Catherine G. Reyes, [a] Jörg Baller, [a] Takeaki Araki *[b] and Jan P. F. Lagerwall *[a]

Received 6th May 2019,
Accepted 11th June 2019

DOI: 10.1039/c9sm00921c

rsc.li/soft-matter-journal

Phase separation in mixtures forming liquid crystal (LC) phases is an important yet under-appreciated phenomenon that can drastically influence the behaviour of a multi-component LC. Here we demonstrate, using polarising microscopy with active cooling as well as differential scanning calorimetry, that the phase diagram for mixtures of the LC-forming compound 4′-*n*-pentylbiphenyl-4-carbonitrile (5CB) with ethanol is surprisingly complex. Binary mixtures reveal a broad miscibility gap that leads to phase separation between two distinct isotropic phases *via* spinodal decomposition or nucleation and growth. On further cooling the nematic phase enters on the 5CB-rich side, adding to the complexity. Significantly, water contamination dramatically raises the temperature range of the miscibility gap, bringing up the critical temperature for spinodal decomposition from ~ 2 °C for the anhydrous case to >50 °C if just 3 vol% water is added to the ethanol. We support the experiments with a theoretical treatment that qualitatively reproduces the phase diagrams as well as the transition dynamics, with and without water. Our study highlights the impact of phase separation in LC-forming mixtures, spanning from equilibrium coexistence of multiple liquid phases to non-equilibrium effects due to persistent spatial concentration gradients.

1 Introduction

Many aspects of research in liquid crystals (LCs)—liquids of anisotropic molecules (mesogens) that spontaneously develop long-range order in molecular orientation—and essentially all commercial applications, utilise mixtures containing multiple components. Even basic consequences of this mixing, like equilibrium phase separation, are frequently overlooked. An exception is the phase separation which occurs in the context of polymer-dispersed liquid crystals (PDLCs), as it is this phenomenon that induces the heterogeneous structure characteristic of PDLCs.[1] Phase separation in LC–polymer mixtures has thus been thoroughly studied, experimentally[2–4] and theoretically.[5–10]

For LC mixtures of exclusively low molar mass components the situation is different. It is not uncommon to see reports of a single clearing temperature of multicomponent mixtures such as E7, which develops the nematic LC phase (exhibiting no long-range order beyond the orientational one). This neglects the extension of the first-order nematic–isotropic transition over a significant temperature range, within which the two phases coexist in equilibrium. Even less attention is given to the fact that the compositions of the two coexisting phases can be very different, and that spatial concentration gradients induced by phase separation remain for long times. The consequences are significant, not least if functional molecules such as a chiral dopant, reactive monomer, photoinitiator or dye are part of the mixture.

When working with mixtures it is therefore generally advisable to avoid first-order transitions and the resulting phase separation. This may not be possible, however, for instance when an LC and an organic solvent are processed together during microfluidic preparation of multiple emulsions,[11–16] printing of solvent-dissolved LCs,[17,18] or in the formation of LC-core filled polymer fibres.[11,19–22] Since the current trend in soft matter and LC research to advance flexible and responsive soft devices and composites renders such procedures popular, solvent-induced phase separation needs to be considered. In some cases, the phase separation may be helpful, as in the study of LC-based gels,[23,24] and it might find technical use in applications that take advantage of the behavior of LCs with incorporated isotropic droplets.[25]

Here we establish the phase diagram of, arguably, the most studied mesogenic compound, 4′-*n*-pentylbiphenyl-4-carbonitrile (5CB), and the equally common solvent ethanol, finding a much

[a] *Physics and Materials Science Research Unit, University of Luxembourg, 162a, Avenue de la Faencerie, L-1511, Luxembourg. E-mail: jan.lagerwall@lcsoftmatter.com*
[b] *Department of Physics, Kyoto University, Kitashirakawa-Oiwakecho, Sakyo-ku, Kyoto 606-8502, Japan. E-mail: araki.takeaki.5a@kyoto-u.ac.jp*

† Electronic supplementary information (ESI) available: DSC data and analysis for 5CB–anhydrous ethanol and 5CB–aqueous ethanol mixtures, detailed heating and cooling analysis and fast-forwarded POM movies of significant 5CB–ethanol mixtures. See DOI: 10.1039/c9sm00921c

richer phase diagram than anticipated. We identify a large miscibility gap that causes two distinct isotropic phases with different compositions to coexist. The phase separation takes place *via* spinodal decomposition or nucleation and growth, depending on the mixture composition. (For readers unaccustomed to these concepts, a summary is provided in the ESI.†) Significantly, a small fraction of water raises the temperature range of isotropic–isotropic phase separation by several tens of degrees. This gives the phase separation strong practical relevance since water may enter mesogen–solvent mixtures through condensation from humid air due to cooling as the solvent evaporates. We support our experimental findings with a theoretical treatment and numerical simulations that qualitatively reproduce the observed phase diagrams and the dynamics of the phase transitions, also with spatial concentration gradients.

To the best of our knowledge, this is the first combined experimental–theoretical investigation of isotropic–isotropic phase separation in LC mixtures without a polymer component. Coincidentally, while our study was on-going, Serrano *et al.* published the first experimental report describing phase separation in 5CB–solvent mixtures.[26] The solvent in that case was methanol instead of ethanol, and the authors did not consider the effect of water added to the mixture. The Serrano *et al.* phase diagram was based mainly on macroscopic optical observation of samples in cuvettes and they also studied an interesting potential application in extraction of target molecules. Our work is based primarily on polarising microscopy, placing the emphasis on elucidating the phase diagrams in detail, with and without water. We pay particular attention to phenomena where the LC character plays a central role, and we also consider the important practical consequences that the phase separation-induced concentration gradients has for LC research.

2 Results and discussion

The majority of the observations discussed below occur in the supercooled regime, as the melting point of pure 5CB is 24 °C. We avoid crystallisation throughout the study and conduct all experiments on cooling from a fully homogeneous isotropic state, and on re-heating from a suitable low temperature prior to any crystallisation occurring. This is motivated by the fact that 5CB has a very strong tendency for supercooling and that this thus corresponds to practical work with the mixtures. Complementing the texture micrographs below, Supporting Movies SM1–SM8 show the dynamics of all experiments (ESI†).

2.1 5CB in anhydrous ethanol

An overview of all mixture compositions investigated is provided in Table 1, together with the methods used to study each composition. Initial screening of macroscopic samples at room temperature showed that all samples with $\leq$75 mol% 5CB are fully isotropic, whereas the sample with 95 mol% 5CB is predominantly nematic. Isotropic–isotropic phase separation is not observed to occur at room temperature for any fraction of 5CB mixed with anhydrous ethanol. To see the separation in these mixtures, we need to cool them to lower temperatures.

Table 1 Compositions, determined gravimetrically, of mixtures of 5CB and anhydrous ethanol, together with the techniques used to investigate each (Macro = macroscopic observation; POM = Polarising Optical Microscopy; DSC = Differential Scanning Calorimetry). An asterisk in the first two columns signifies that the composition was determined on the sample used for DSC after the final measurement; no asterisk indicates that the composition was determined at the point of mixture preparation

Mol% 5CB	Mass% 5CB	Macro.	POM	DSCs
9.9	37.3	Y	Y	N
14.8*	48.5*	N	N	Y
18.6	55.3	N	Y	Y
27.8*	67.6*	N	N	Y
29.0	68.9	N	Y	N
30	69.8	Y	N	N
40	78.3	Y	N	N
49.2*	84.8*	N	Y	Y
77.2*	94.8*	N	Y	Y
95	99.1	Y	Y	N

2.1.1 The isotropic–isotropic coexistence on cooling. The two anhydrous mixtures investigated that show spinodal decomposition between two compositions of isotropic phase are those with 18.6 mol% (ESI† SM1) and 29.0 mol% 5CB (ESI† SM2). In accordance with the phase diagram presented in Fig. 1, a clear example of isotropic–isotropic phase separation becomes visible close to −4.7 °C for the 18.6 mol% mixture on cooling (Fig. 2a–d). As the separation generates a strongly scattering texture when viewed through the POM with a first-order λ plate inserted (Fig. 2a) or by removing one polariser (Fig. 2d), the isotropic–isotropic phase separation appears to take place largely *via* spinodal decomposition. The characteristic bicontinuous texture can be seen well in ESI† SM3. We note, however, that the original isotropic phase persists within certain areas of the capillary even on cooling further to a slightly lower temperature (Fig. 2b–d). Moreover, the onset temperature of phase separation is somewhat lower in the POM investigation than what the phase diagram in Fig. 1 would suggest; those transition temperatures are established from Differential Scanning Calorimetry (DSC) data (see ESI†).

Since the temperature control equipment is of high quality and has been calibrated, we do not believe that this discrepancy is due to experimental error. Instead, we attribute the ''too low'' transition temperature during POM investigation as well as the unexpected combination of spinodal decomposition and supercooled original phase to significant spatial concentration gradients that persist within the sample, following phase separation occurring prior to the POM experiments. The capillaries used for these experiments are 100 μm thick, 1 mm wide and about 3 cm long, hence the sample volume is so large that removal of concentration gradients by diffusion takes long time. This means that we have regions in the capillary with lower 5CB content than 18.6 mol% as well as regions where the 5CB content is higher. Regions with less 5CB retain a uniform isotropic phase that is stable at lower temperatures, while regions with higher 5CB content cross the spinodal curve on cooling and separate into two new isotropic phases. This situation allows

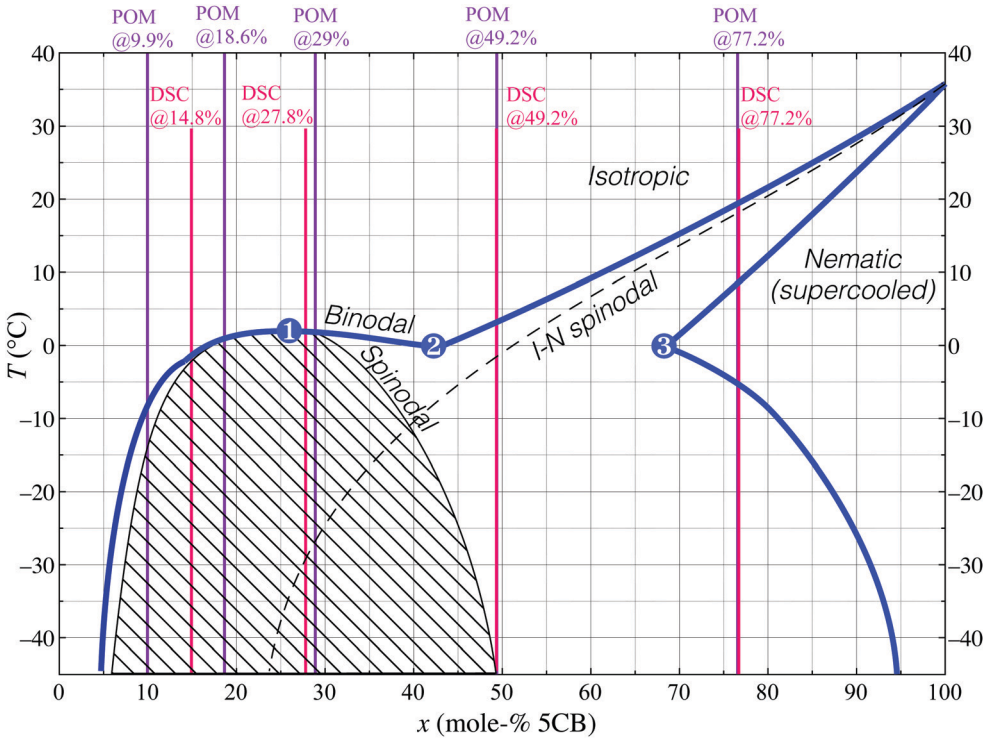

Fig. 1 Experimental phase diagram for 5CB and anhydrous ethanol, established by a combination of POM (for phase determination; at compositions indicated with purple vertical lines) and DSC (for transition temperatures; at compositions indicated by red vertical lines). Three points of special importance are indicated: (1) the critical point of spinodal decomposition, (2) the eutectic point of the intermediate composition isotropic phase, which is also the minimum temperature of equilibrium isotropic–isotropic phase coexistence, and (3) the lowest 5CB content possible for 100% nematic phase.

significant supercooling of the original isotropic phase and explains the discrepancies from the DSC experiments, which were done using aluminum pans providing better heat conduction and less spreading-out of the sample.

2.1.2 Nematic–isotropic coexistence on cooling. The 9.9 mol% 5CB mixture (SM4 and Fig. S2, ESI†) does not show isotropic–isotropic separation, as indicated in Fig. 1. On cooling, the nematic phase nucleates directly from the homogeneous isotropic phase, and on subsequent heating the nematic droplets disappear without any trace of additional isotropic phase. The isotropic phase at 9.9 mol% 5CB is stable down to temperatures below that of the eutectic point (2) in Fig. 1, which is the lowest temperature at which isotropic–isotropic separation is possible.

Unlike the simplicity of one nematic and one isotropic phase in coexistence at 9.9 mol% 5CB, the situation on cooling the 18.6 mol% and 29 mol% mixtures increases in complexity. First, for both mixtures one of the new isotropic phases that previously emerged begins changing into nematic at −7.2 °C. These droplets become birefringent and develop a typical nematic schlieren texture (Fig. 2e and f). Once again, the transition temperature appears too low in the POM experiments, as the minimum temperature of equilibrium isotropic phase at intermediate composition (the eutectic point, (2)) should be around 0 °C according to Fig. 1. We interpret this as a sign of the now unstable isotropic phase being supercooled to temperatures below point (2), allowed until the isotropic–nematic spinodal transition is met, here thus at −7.2 °C.

Cooling further we eventually see isotropic droplets nucleate within large domains of nematic phase (Fig. 2g and h). These tiny isotropic droplets tend to line up as chains in order to minimise distortion energy within the surrounding nematic phase.[27] Small nematic domains, in contrast, simply shrink, the isotropic surrounding growing in prominence. Since the temperature is now below that of the point labeled (3) in Fig. 1, the nematic phase must continuously increase its 5CB content on cooling. Small nematic droplets achieve this easily by exchanging with their immediate isotropic surrounding, shrinking somewhat in the process. For larger nematic domains (on the order of several hundreds of microns wide) the border to the isotropic phase is too far away, hence many small isotropic droplets with greater ethanol content nucleate within the nematic domain.

It is important to realise that the isotropic phase of these tiny droplets dispersed in the nematic domains is identical in composition to the background isotropic phase, *i.e.*, it is on the far left side of the coexistence region in the phase diagram. The spatial separation from the background isotropic phase that we observe is of purely kinetic origin, resulting from the nucleating isotropic droplets being trapped within the large nematic phase domains. If the temperature is held constant, then these isotropic droplets gradually move to the edge of the domain where they merge with the surrounding, but this can take several hours or days.

For mixtures containing fractions of 5CB in anhydrous ethanol of about 50 mol% (ESI† SM5) or greater—thus the

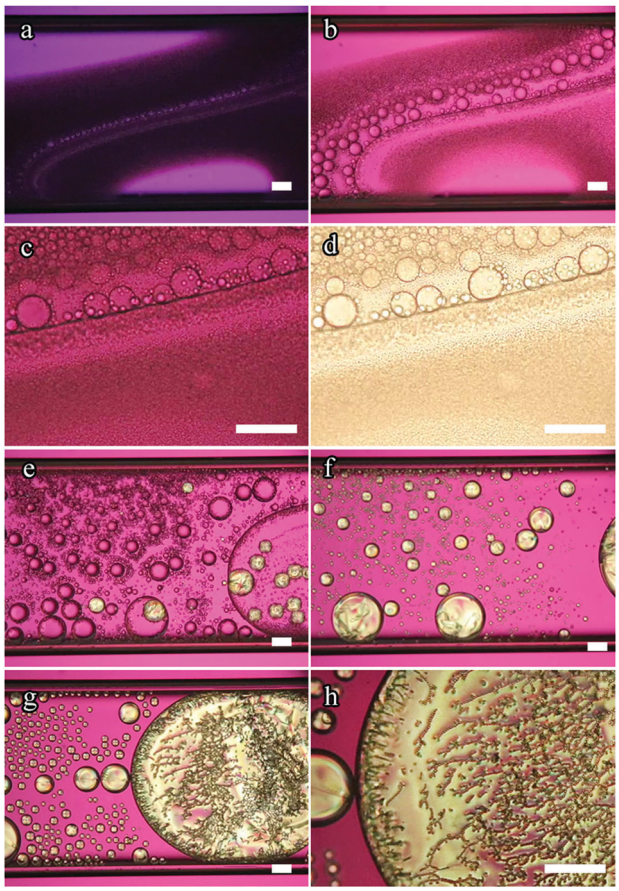

Fig. 2 POM images of the 18.6 mol% 5CB mixture in a 100 μm thick flat capillary on cooling from the uniform isotropic phase (see also ESI† SM1). Two new phases emerge *via* spinodal decomposition at roughly −4.5 °C, (a). Boundaries between the original and new isotropic phases are visible through crossed polarisers with first-order λ plate (pink background), (b and c), or without polarisers, (d). The nematic phase nucleates from one of the new isotropic phases between −7.2 °C, (e), and −8.0 °C, (f). Isotropic droplets in chains nucleate below −4.8 °C, (g) in the nematic domains, and continually accumulate (−16.5 °C, h). The 20 and 29 mol% samples show the same features on cooling (see ESI†). Scale bars: 100 μm.

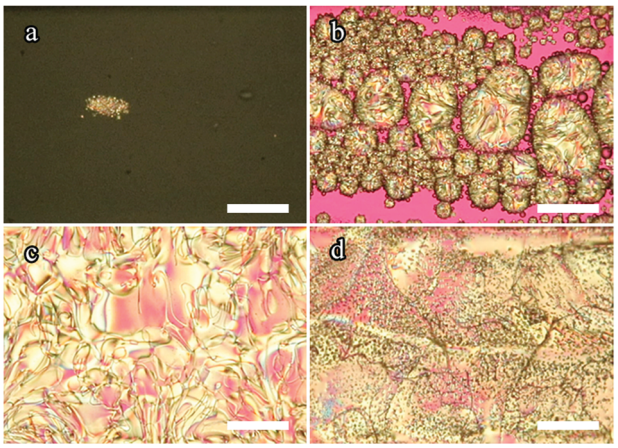

Fig. 3 POM images of the 49.2 mol% 5CB mixture in a 100 μm thick flat capillary on cooling from uniform isotropic phase, with nematic phase entering just below 0 °C (see also ESI† SM5). Image (a) was taken at −0.7 °C. The nematic phase grows in prominence when cooled to −4.8 °C, (b). At −5.5 °C, (c), the nematic phase fills the capillary almost entirely. If the sample is cooled to −7.8 °C the 5CB content of the nematic phase increases and chains of small isotropic droplets nucleate, (d). Qualitatively, the 77.2 mol% sample exhibits similar features (see ESI† for details). Pink background is due to a first-order λ plate inserted. Scale bars: 100 μm.

right half of the phase diagram in Fig. 1, encompassing the ordinary nematic–isotropic phase separation—the nematic phase nucleates directly from the uniform isotropic phase (Fig. 3). In the phase diagram we are now to the right of the eutectic point of the isotropic phase with intermediate composition, hence the two-phase region we encounter on cooling is not between two new isotropic phases, but between the original isotropic phase and the nematic phase.

For the mixture containing 77.2 mol% 5CB (ESI† SM6), the nematic phase nucleates from the uniform isotropic phase at roughly 16 °C. As this mixture has more 5CB than the composition at point 3 in the phase diagram, the cooling experiment crosses the range in which the nematic is the sole thermodynamically stable phase. According to Fig. 1 this range should start at about 8 °C, yet a minority isotropic phase still remains until 5 °C where the full sample becomes nematic. We attribute this to the concentration gradients that built up during prior cooling experiments, and non-equilibrium phenomena while these are slowly evened out. For the same reason, it is not until about −11 °C that we see the first isotropic droplets nucleate within the nematic phase. The lower boundary of the stable nematic phase range in Fig. 1 for this mixture is higher, about −5 °C, as established by DSC.

2.1.3 Nematic–isotropic and isotropic–isotropic coexistence on heating. For the 18.6 mol% sample, upon reheating, the isotropic phase droplets within large nematic domains start to disappear as we approach point (3) in the phase diagram (Fig. 4a). At about −7 °C an isotropic–isotropic phase separation is observed, as small nematic droplets turn isotropic, yet remain distinct from the background isotropic phase. This new isotropic phase is also seen as a ribbon growing around the large nematic domains (Fig. 4b). The new phase should have the eutectic composition of point (2), as it is the lowest-temperature isotropic phase distinct from the isotropic phase on the left side of the phase coexistence regime.

However, as is frequently observed during the POM investigations, there is again a considerable transition temperature difference compared to the results seen from the DSC experiments. We consider this another piece of evidence of the impact of the local concentration gradients established by the phase separation at low temperatures. These non-equilibrium phenomena mean that it is very challenging to draw quantitative conclusions regarding transition temperatures from experiments on mixtures in large-scale samples such as capillaries.

As we heat further, the composition of the new isotropic phase rapidly decreases its 5CB content, moving along the boundary from (2) to (1) in Fig. 1. Since the overall mixture composition has only 18.6 mol% 5CB, according to the phase diagram, we ought to only have the two isotropic phases

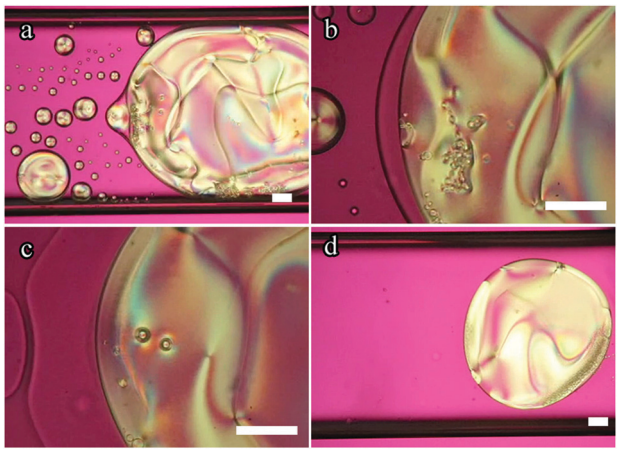

Fig. 4 POM images of the 18.6 mol% 5CB mixture in a 100 μm thick flat capillary on heating. Between roughly −6.3 °C and −7.0 °C, (a and b), the isotropic droplets within the nematic domains disappear and a new isotropic phase begins replacing the small nematic droplets as well as making a boundary around the large nematic domains. At −0.7 °C the two isotropic domains merge, (c), leaving the remaining nematic domains to clear last, (d). Qualitatively, the 29 mol% sample exhibits the same features on heating (see ESI† for details). Pink background is due to a first-order λ plate inserted. Scale bars: 100 μm.

coexisting during this process. Indeed, this is what we saw earlier when cooling at these temperatures. However, as is shown in Fig. 4c and d, it is not the case on heating, where nematic phase remains past the temperature where the two isotropic phases coalesce to one uniform isotropic phase. The fact that on heating we see a persistent nematic phase even up to +10 °C is yet another strong indication of the significant concentration gradients occurring within the capillary sample. Some regimes clearly have a much higher 5CB content than the overall 18.6 mol% for a long time. The isotropic–isotropic phase coexistence disappears slightly above 0 °C (Fig. 4c), as the temperature is now in the uniform isotropic phase range for a large composition range, apparently spanning the gradients existing within the sample. Similar observations were made for the 29 mol% 5CB mixture (see ESI† for details).

Notably, the mixtures containing 49.2 mol% and 77.2 mol% do not show phases coexisting longer than they should upon heating, like the 18.6 mol% and 29 mol% mixtures do. Since there is no isotropic–isotropic coexistence to begin with, the nematic phase, once all the isotropic droplets have disappeared, and as expected from Fig. 1, clears uniformly to a single isotropic phase.

Of key importance for understanding the origin of the persistent concentration gradients is the very large width of the miscibility gap: below −10 °C the nematic phase has more than 80 mol% 5CB while the isotropic has less than 10 mol% 5CB, regardless of what the overall sample composition is. If the samples would have been kept for several days at a temperature where the full sample is isotropic, possibly the concentration gradients would have been evened out and a behaviour more in line with the phase diagram (and with the DSC experiments) would have been observed in the POM investigation of the capillary.

2.2 The effect of water impurity: 5CB in aqueous ethanol

While bottles of spectroscopic grade anhydrous ethanol having a purity of ≥99.8% can be purchased from many distributors, it is not uncommon to work with 95–97% ethanol, where the dominant impurity is typically water. It is thus of interest to investigate whether the phase diagram in Fig. 1 changes significantly if the ethanol is contaminated with a small fraction of water. For this reason, we also examine several mixtures of 5CB mixed with a solvent (referred to as "aqueous ethanol" from this point on) consisting of 96 mass% anhydrous ethanol and 4 mass% deionized water, corresponding to roughly 97 and 3 vol%, respectively. An overview of these mixture compositions, with the methods used to study each, is shown in Table 2. We prepare a bulk mixture of this aqueous ethanol rather than using commercial 97 vol% ethanol, so as to avoid the influence of other unknown impurities (such as methanol or benzene) on the phase diagram.

While all mixtures listed in Table 2 examined using the POM and temperature control stage qualitatively show the same phase behaviour as the mixtures containing only 5CB and anhydrous ethanol, a crucial difference concerns the onset temperatures for isotropic–isotropic phase separation. In contrast to the mixtures discussed in Section 2.1.1, mixtures using aqueous ethanol with a 5CB content in the range 10–20 mol% show macroscopically visible separation between immiscible isotropic phases at room temperature, as shown in Fig. 5. The photos show three mixtures containing 9.6 mol%, 21 mol% and 51 mol% 5CB, respectively, in aqueous ethanol, observed close to room temperature (~23 °C). The figure demonstrates that increasing the fraction of 5CB has the effect of raising the isotropic–isotropic phase separation line towards the concave meniscus line until a critical concentration of 5CB is met (based on the approximate phase diagram in Fig. 6, about 43 mol%). At 51 mol% 5CB only one isotropic phase is stable at room temperature, as evidenced through a macroscopically uniform transparent liquid with no line below the meniscus to the air. Aqueous ethanol mixtures containing 77 mol% and 85 mol% 5CB follow the same trend, appearing uniformly isotropic at room temperature as well.

When observed in capillaries through the POM with a λ plate inserted, the mixtures with 9.6 mol% and 21 mol% 5CB show several boundary lines confirming the separation of two isotropic liquid phases (ESI† SM7), even after heating to above the

Table 2 Compositions, determined gravimetrically, of the mixtures of 5CB in aqueous ethanol (97 vol%), together with the techniques used to investigate each (Macro = macroscopic observation; POM = Polarising Optical Microscopy; DSC = Differential Scanning Calorimetry)

Mol% 5CB	Mass% 5CB	Macro.	POM	DSC
9.6	38	Y	N	N
11	41	N	N	Y
21	60	Y	Y	N
32	73	N	N	Y
51	86	Y	N	N
74	94	N	N	Y
77	95	Y	Y	N
85	97	Y	Y	N

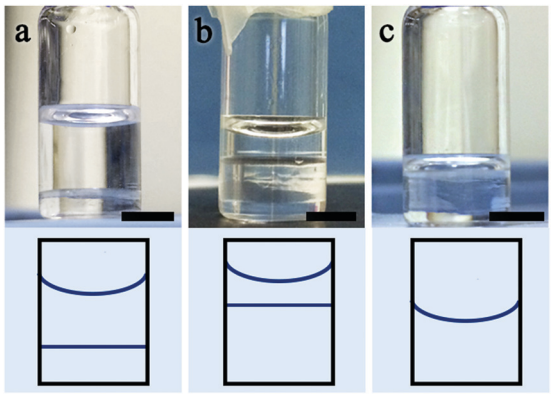

Fig. 5 Macroscopic photographs at room temperature of three mixtures of 5CB with ethanol to which 3 vol% water was added. Isotropic–isotropic phase separation is seen in the first two vials, with 9.6 mol% 5CB (a), and 21 mol% 5CB (b), respectively. The third vial, containing a 51 mol% 5CB mixture, has a single isotropic phase. Sketches showing the change in the isotropic–isotropic separation line relative to the meniscus with air qualitatively reflect the phase diagram in Fig. 6 as the composition of 5CB moves from the left side (lower 5CB fraction) to the right side (higher 5CB fraction). Scale bars: 0.5 cm.

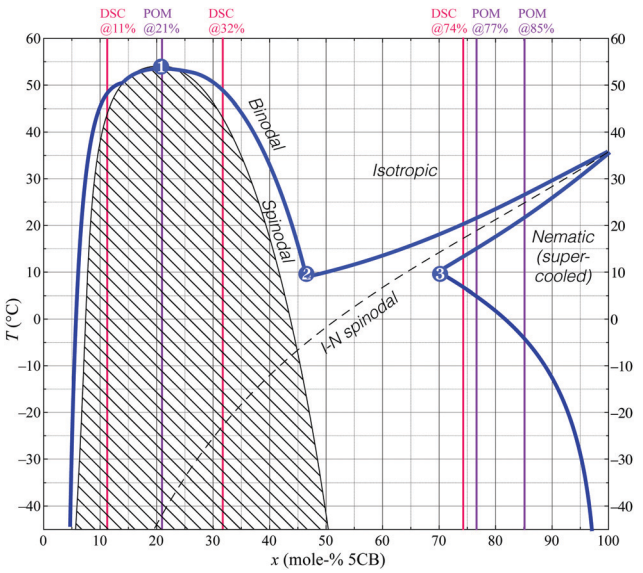

Fig. 6 Slice of the ternary experimental phase diagram for the 5CB–ethanol–water system; 3 vol% water is added to anhydrous ethanol to create a 97 vol% ethanol–water mixture for mixing with 5CB. The same three points of interest as in Fig. 1 have been highlighted, and DSC and POM measurement compositions are indicated in the same way.

clearing temperature of pure 5CB (35 °C). In fact, it is only after the capillary samples are heated to roughly 45 °C that the coexisting isotropic phases merge to a single phase.

What does the introduction of water mean for the phase diagram between 5CB and ethanol? For simplicity, in addition to not varying the pressure of the 5CB–ethanol–water system, we do not vary the fraction of water added to the mixtures. Thus, while our revised phase diagram shown in Fig. 6 only demonstrates a slice of the full ternary diagram, it is enough to conclude that adding at least 3 vol% of water to the ethanol dramatically increases the temperature at which the coexisting isotropic phases are stable, to the left of the eutectic point initially seen in Fig. 1. This is confirmed by POM and DSC investigations of selected mixtures, complementing the macroscopic observations in Fig. 5. DSC traces on cooling mixtures of the same composition as in Fig. 5(a) and (b) clearly reveal a highly reproducible peak at 44 °C (see ESI†) that signifies the isotropic–isotropic phase separation, most likely by spinodal decomposition. The transition to a nematic phase is also raised compared to the corresponding mixtures with anhydrous ethanol, two partially overlapping peaks repeatedly being detected at 9 °C and 7 °C, respectively. We attribute these peaks to the passing of the eutectic point (2) and the isotropic–nematic spinodal, respectively. The DSC measurements conform well with the heating and cooling observations made at the POM using capillaries containing similar mixture compositions.

As for the mixture in Fig. 5(c), containing 51 mol% 5CB, the DSC traces indicate that an isotropic–nematic transition occurs between 14 °C and ~9 °C on cooling. This is in rather good agreement with the nucleation of nematic seen through the POM for the 51 mol% aqueous ethanol mixture from ~6 °C. The significant difference in the DSC traces for this mixture compared to the two mixtures with less 5CB indicates that this mixture has a composition to the right of the eutectic point (2), whereas the former ones are both to the left of that point.

Considering that the critical temperature of spinodal decomposition is far below room temperature for the mixture with anhydrous ethanol, it is interesting to note that the critical temperature for isotropic–isotropic phase separation reported by Serrano *et al.* for 5CB–methanol mixtures was located at about 25 °C.[26] As methanol has a boiling point about 14 °C lower than ethanol, it is not obvious why the temperature of phase separation would be much higher with methanol as solvent than with ethanol. While Serrano *et al.* used HPLC grade methanol, thus taking care not to introduce any water deliberately, the low boiling point of methanol may perhaps have led to some evaporation-induced cooling and water condensation from the air[28] during sample preparation, thus bringing a small amount of water into the mixtures inadvertently. Considering the strong effects of water in the ethanol–5CB system seen by comparing Fig. 1 and 6, this might be a means of reconciling the large differences in temperature ranges between our study and that of Serrano *et al.*

2.3 Theory and simulations

2.3.1 Phase diagram. In order to corroborate the experimental observations theoretically and to better understand the origin of the strong sensitivity to water contamination, we also study phase separation in LC–solvent mixtures numerically.[7–9,29] First, we consider the free energy of binary mixtures of an LC-forming (mesogenic) compound and a one-component solvent.[10,30,31] We employ two order parameters $\phi(\mathbf{r},t)$ and $q_{ij}(\mathbf{r},t)$, which vary in space ($\mathbf{r}$) and time (t). The parameter ϕ is the volume fraction of the mesogenic component and q_{ij} is the orientational order per volume. They are defined with $f(\mathbf{r},\mathbf{u},t)$, which is the probability distribution of mesogens for

orientation $\mathbf{u}$ and position $\mathbf{r}$, respectively. For the distribution of orientations at a certain position $\mathbf{r}$, we have:[29,32]

$$\phi(\mathbf{r},t) = v\int \mathrm{d}\mathbf{u} f(\mathbf{r},\mathbf{u},t), \tag{1}$$

$$q_{ij}(\mathbf{r},t) = v\int \mathrm{d}\mathbf{u} f(\mathbf{r},\mathbf{u},t)\left(\mathbf{u}_i\mathbf{u}_j - \frac{1}{3}\delta_{ij}\right). \tag{2}$$

Here $\mathbf{u}$ is the unit vector along a mesogen, and v is its volume. The indices i and j stand for the spatial coordinates x, y, and z. The repeated indices are assumed to be summed over. From eqn (1) and (2), the probability distribution can be expanded with ϕ and q_{ij} as

$$f(\mathbf{r},\mathbf{u}) = \frac{1}{4\pi v}\left[\phi(\mathbf{r}) + \frac{15}{2}q_{ij}(\mathbf{r})\left(u_iu_j - \frac{1}{3}\delta_{ij}\right)\right]. \tag{3}$$

Knowing f, we obtain the (rescaled) entropy from the translational and rotational degrees of freedom of mesogens as:

$$\mathscr{S}_{\mathrm{meso}} = -\int \mathrm{d}\mathbf{r}\int \mathrm{d}\mathbf{u} f(\mathbf{r},\mathbf{u})\{\ln[vf(\mathbf{r},\mathbf{u})] - 1\}, \tag{4}$$

where we for simplicity have set the Boltzmann constant to unity. By substituting eqn (3) into eqn (4) and integrating it over $\mathbf{u}$ with the isotropic approximation, we can describe $\mathscr{S}_{\mathrm{meso}}$ as a functional of ϕ and q_{ij} as,

$$\mathscr{S}_{\mathrm{meso}} \approx -\frac{1}{v}\int \mathrm{d}r\left[\phi\ln\phi + \frac{a}{2\phi}q_{ij}q_{ji} - \frac{b}{3\phi^2}q_{ij}q_{jk}q_{ki} + \frac{c}{4\phi^3}(q_{ij}q_{ji})^2\right], \tag{5}$$

where the numerical constants are calculated as $a = 15/2$, $b = 225/14$, $c = 1125/28$.[29] Then, the total entropy $\mathscr{S}$ is given by

$$\mathscr{S} = \mathscr{S}_{\mathrm{meso}} - \frac{1}{v'}\int \mathrm{d}\mathbf{r}(1-\phi)\ln(1-\phi). \tag{6}$$

The second term of the right hand side in eqn (6) represents the translational entropy of the solvent molecule, whose volume is ν'.

The energy $\mathscr{E}$ is also given by a functional of ϕ and q_{ij} as

$$\begin{aligned}\mathscr{E} = \frac{1}{v}\int \mathrm{d}\mathbf{r}\Big[&J\phi(1-\phi) - \frac{\varepsilon}{2}q_{ij}q_{ji} \\ &+ \frac{K}{2}(\nabla\phi)^2 + \frac{L}{2}\left(\nabla_k q_{ij}\right)^2 + W\left(\nabla_i\phi\nabla_j q_{ij}\right)\Big],\end{aligned} \tag{7}$$

where J represents the isotropic part of the interaction energy between the mesogens and solvent molecules, and ε is the anisotropic part of the interaction between the mesogens. The remaining terms represent the energy costs due to the gradients of ϕ and q_{ij}. Their coefficients are estimated by $K = Jv^{2/3}$, $L = \varepsilon v^{2/3}$ and $W = \varepsilon v^{2/3}$. These three terms are related to the interfacial tension, the elasticity of the nematic phase and the anchoring effect of the director field (describing the orientational order) on the interfaces, respectively.

The free energy is given by

$$\mathscr{F} = \mathscr{E} - T\mathscr{S}. \tag{8}$$

The concentration field and the nematic order parameter are determined to minimise $\mathscr{F}$ at each temperature T. We note that ϕ is a conserved variable, while q_{ij} is not. When two phases (1 and 2) coexist, their concentrations and nematic order parameters are determined by the following conditions.

$$\left.\frac{\delta\mathscr{F}}{\delta\phi}\right|_{\phi=\phi_1,q=q_1} = \left.\frac{\delta\mathscr{F}}{\delta\phi}\right|_{\phi=\phi_2,q=q_2}, \tag{9}$$

$$\left.\frac{\delta\mathscr{F}}{\delta q_{ij}}\right|_{\phi=\phi_1,q=q_1} = \left.\frac{\delta\mathscr{F}}{\delta q_{ij}}\right|_{\phi=\phi_2,q=q_2} = 0 \tag{10}$$

In a pure mesogenic system (ϕ = 1), this free energy is consistent with the Landau-de Gennes free energy. Thus, the isotropic–nematic transition temperature T^0_{IN} is given by

$$T^0_{\mathrm{IN}} = \frac{\varepsilon}{a - b^2/(27c)}. \tag{11}$$

If the concentration is homogeneous, the isotropic–nematic transition temperature is given by a function of ϕ as,

$$T_{\mathrm{IN}}(\phi) = T^0_{\mathrm{IN}}\phi. \tag{12}$$

When the nematic order is zero, on the other hand, eqn (8) reproduces the Flory–Huggins type free energy, describing the isotropic–isotropic phase separation. Its critical point is given by

$$\phi_{\mathrm{c}} = 1\Big/\left(1 + \sqrt{v/v'}\right), \tag{13}$$

$$T_{\mathrm{c}} = 2J\left(1/\sqrt{v} + 1/\sqrt{v'}\right)^{-2}. \tag{14}$$

Also, the spinodal temperature T_{sp} for the isotropic–isotropic phase separation is given as a function of ϕ by

$$T_{\mathrm{sp}}(\phi) = \frac{2J}{1/(\phi v) + 1/[(1-\phi)v']}. \tag{15}$$

In our model, only two parameters (J and ν/ν') determine the shape of the phase diagram. In other words, we can obtain the phase diagram if we know the critical point (ϕ_{c},T_{c}).

Fig. 7 shows a typical phase diagram of a binary mixture containing the mesogenic component. It is obtained solving eqn (9) and (10) numerically. Here we set $T_{\mathrm{c}}/T^0_{\mathrm{IN}}$ = 0.8 and ϕ_{c} = 0.39 (J/T^0_{IN} = 1.06 and ν/ν' = 2.5) (black curves). Note that, in order to improve the comparison with the experimentally established phase diagrams, the horizontal axis represents the molar fraction $\varphi = (\phi/\nu)/[\phi/\nu + (1-\phi)\nu']$, not the volume fraction ϕ.

The calculated phase diagram is similar with the experimental results. Around $\phi \approx \phi_{\mathrm{c}}$, the coexistence of the two isotropic liquids can be observed. This isotropic–isotropic coexistence is due to the isotropic part J of the interaction energy between the two components. When the average concentration is large enough, on the other hand, an isotropic phase coexists with a nematic phase. The latter coexistence is realised by the nematic ordering. In Fig. 7, we also explore changing T_{c} with fixing ϕ_{c} $T_{\mathrm{c}}/T^0_{\mathrm{IN}}$ = 0.9 (red curves) and $T_{\mathrm{c}}/T^0_{\mathrm{IN}}$ = 1.05 (blue curves). The phase diagram can be tuned with these two parameters.

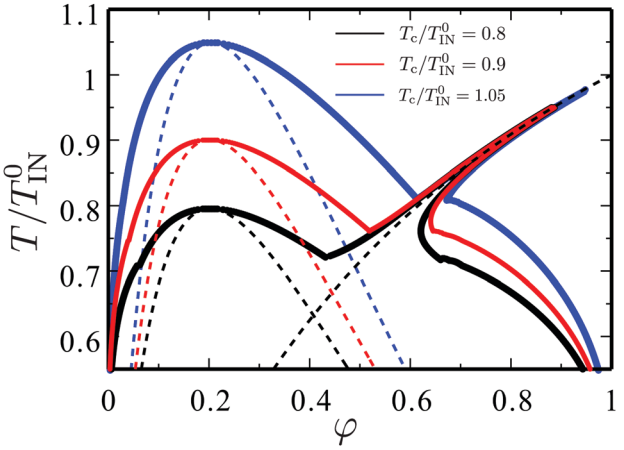

Fig. 7 Theoretical phase diagram for the LC–solvent mixtures. The horizontal axis represents the molar fraction $\varphi = (\phi/\nu)/[\phi/\nu + (1-\phi)\nu']$ of the mesogenic compound. The critical point for the isotropic–isotropic phase separation is tuned between the three curves: $T_c/T_{IN}^0 = 0.8$ (black), $T_c/T_{IN}^0 = 0.9$ (red) and $T_c/T_{IN}^0 = 1.05$ (blue), respectively. The spinodal curve for the isotropic–isotropic phase separation (eqn (15)) is shown for all cases, and the isotropic–nematic transition temperature without prior phase separation (eqn (12)) is shown for $T_c/T_{IN}^0 = 0.8$.

2.3.2 Dynamic equations. Next we describe the time developments of the two order parameters.[7,33–36] Instead of $q_{ij}(\mathbf{r})$, we consider the nematic order per molecule $Q_{ij}(\mathbf{r}) = q_{ij}(\mathbf{r})/\phi(\mathbf{r})$ in numerical simulations. Their dynamic equations are given by

$$\frac{D}{Dt}\phi = \frac{Dv}{T}\nabla^2\mu + \theta, \tag{16}$$

$$\frac{D}{Dt}Q_{ij} = Q_{ik}\kappa^a_{kj} - \kappa^a_{ik}Q_{kj} + \frac{1}{\gamma}H_{ij} + \beta\kappa^s_{ij} + \xi_{ij}, \tag{17}$$

where $D/Dt(= \partial/\partial t + \mathbf{v}\cdot\nabla)$ is the Lagrange time derivative with the hydrodynamic flow $\mathbf{v}$. The chemical potential is given by $\mu = \delta\mathscr{F}/\delta\phi$ and $H_{ij} = -[\delta\mathscr{F}/\delta Q_{ij} - (\delta\mathscr{F}/\delta Q_{kl})\delta_{kl}\delta_{ij}/3]$ is the molecular field. The parameters κ^s_{ij} and κ^a_{ij} are the symmetric and asymmetric parts of the velocity gradient tensor $\nabla_i v_j$, respectively, and D and γ are the diffusion constant and the rotational viscosity of the mesogenic component, respectively. Finally, β is the so-called flow-alignment parameter and θ and ξ_{ij} represent the thermal noises for ϕ and Q_{ij}, respectively.[7,37] We ignore the off-diagonal kinetic coefficients for simplicity in this study.

The hydrodynamic equation is given by,

$$-\phi\nabla_i\mu + \nabla_j(Q_{ik}H_{kj} - H_{ik}Q_{kj}) + Q_{jk}\nabla_i H_{kj} - \beta\nabla_j H_{ij} - \nabla_i p + \eta\nabla^2\mathbf{v} = 0 \tag{18}$$

Here p is the pressure, which is imposed to satisfy the incompressible condition $\nabla\cdot\mathbf{v} = 0$, and η is the viscosity.[7]

We numerically solve eqn (16)–(18) with explicit Euler schemes and MAC method.[7,33] The space and time are scaled by $d(\equiv\nu^{1/3})$ and $t_0(\equiv d^2/D)$. The time increment is $\Delta t = 0.005t_0$. We set $\gamma = \eta = 0.2T/(Dd)$ and $\beta = 0.1$ in this work. The simulations are carried out in a two dimensional lattice (1024×256) with periodic boundary condition.

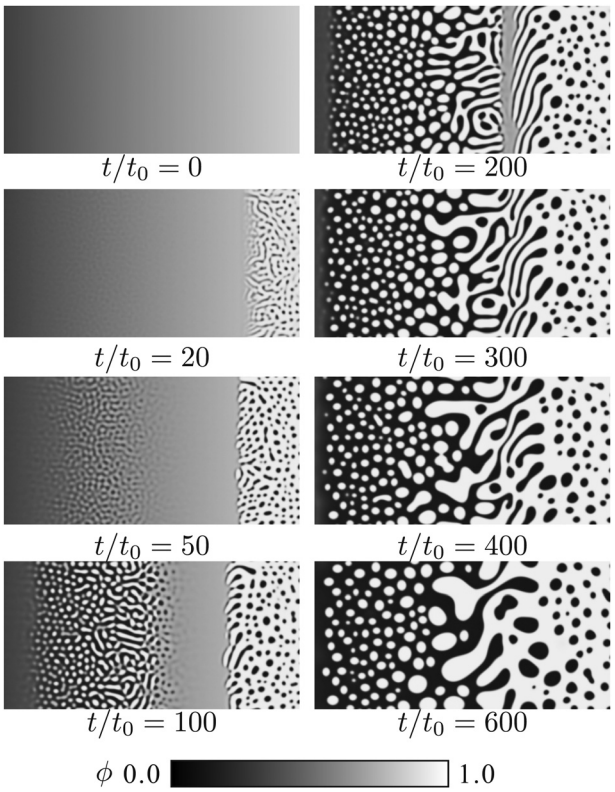

Fig. 8 Simulated pattern evolution of the concentration field ϕ during the phase separation under a concentration gradient. The mesogen–solvent mixture corresponds to the black curve in Fig. 7 ($T_c/T_{IN}^0 = 0.8$). The quenched temperature is $T/T_{IN}^0 = 0.65$.

2.3.3 Numerical results. Fig. 8 shows snapshots from the evolution of the concentration, whereas the corresponding pictures of the nematic field Q_{xy} are shown in Fig. 9. The quenched temperature is $T_c/T_{IN}^0 = 0.8$, which corresponds to the black curve in Fig. 7. In order to consider the phase separation under a concentration gradient,[38] we prepared an inhomogeneous concentration field as an initial condition. The initial concentration at the two boundaries of the x-direction ($x/d = 1$ and 1024) is $\phi = 0.2$, and that at the centre ($x/d = 512$ and 513) is set to $\phi = 0.8$. In the other regions, the concentration field changes linearly with x. Along the y-direction, the initial concentration field is uniform. In Fig. 8 and 9, only half of the system is shown ($1 \le x/d \le 512$).

It is shown that the phase separation occurs heterogeneously, and a variety of domain patterns are observed. At $t = 0$, we quench the system to $T_c/T_{IN}^0 = 0.65$. After the quenching, interestingly, phase separation starts around mesogen-rich and mesogen-poor regions. In contrast to the situation without initial concentration gradient, phase separation proceeds slowly around $\phi = 0.5$. This behavior reflects the distance between the quenched temperature and the phase separation temperature at each concentration. In the mesogen-rich region, the isotropic–nematic transition occurs prior to the phase separation. This nematic ordering induces the nucleation of mesogen-poor domains. We can see a sharp boundary between the phase separated and mixed regions.

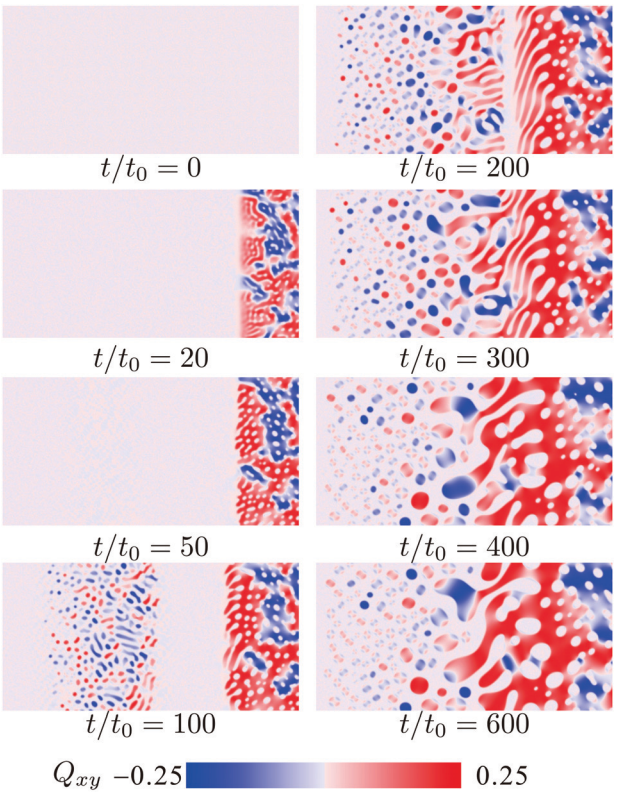

Fig. 9 Simulated pattern evolution of the *xy*-component of the nematic order parameter Q_{xy} during phase separation under a concentration gradient. The mixture is the same as in Fig. 8.

On the other hand, the isotropic–isotropic spinodal decomposition occurs in the mesogen-poor region. In a usual phase separation, the isotropic–isotropic spinodal decomposition leads to a bicontinuous pattern. In this mixture, however, the mesogen-rich domains are formed after the spinodal decomposition, since the phase diagram is asymmetric due to the value of $\nu/\nu(>1)$. After the isotropic–isotropic phase separation, the nematic ordering occurs in the mesogen-rich droplets. As a result, mesogen-rich and mesogen-poor domains are observed simultaneously in the system.

As noted above, the phase separation proceeds slowly around the symmetric concentration. Here bicontinuous patterns are formed. It is known that the bicontinuous domain pattern grows with time more quickly than the droplets pattern, because the hydrodynamic flow enhances the domain growth.[39,40] In the late stage, the domain patterns around the symmetric region can be larger than those around the asymmetric regions.

2.3.4 Phase separation in ternary mixtures. Finally, we discuss the phase behavior in ternary mixtures (mesogenic compound, solvent A and solvent B).[41–43] Their volume fractions are written by ϕ, ϕ_A and ϕ_B, which satisfy $\phi + \phi_A + \phi_B = 1$. In the ternary mixture, the entropy (eqn (6)) is replaced by

$$S = S_{meso} - \int d\mathbf{r}\left[\frac{1}{v_A}\phi_A \ln \phi_A + \frac{1}{v_B}\phi_B \ln \phi_B\right], \quad (19)$$

where v_A and v_B are the volumes of the two solvent molecules.

Also, the isotropic part of the interaction energy (the first term in the right hand side of eqn (7)) is replaced by

$$J\phi(1-\phi) \rightarrow J_A\phi\phi_A + J_B\phi\phi_B + J_{AB}\phi_A\phi_B, \quad (20)$$

where J_A, J_B and J_{AB} represents the interaction energies for the three pairs among the mesogenic compound and the two solvents (A and B).

It is known that the behaviours in the ternary mixture are quite complex, even if all the phases are isotropic. If the affinity between the two solvents is sufficiently good, the ternary mixture can be treated as a pseudo-binary mixture, in which the two solvents behave as a mixed solvent. By expressing ϕ_A and ϕ_B as $\phi_A = (1-\phi)(1-\psi)$ and $\phi_B = (1-\phi)\psi$, a single liquid approximation[41,42] leads to an effective interaction energy

$$J_{eff} = J_A + (J_B - J_A)\psi + J_{AB}\psi(1-\psi), \quad (21)$$

where ψ is the fraction of solvent B in the mixed solvent ($\psi = \phi_B/(\phi_A + \phi_B)$). In the single liquid approximation, ψ is assumed to be constant in space.

Although we have not calculated the exact phase diagram of the ternary mixture, we can understand why a small amount of the third liquid (*i.e.* water in the experiments) changes the phase diagram so drastically. In the experiments, we have not confirmed stable coexistence of three phases, so ethanol and water behave as a co-solvent for 5CB. It is considered that water is a poorer solvent for 5CB in comparison with ethanol ($J_{water} > J_{ethanol}$). Thus, the addition of water enlarges the effective interaction J_{eff} and the mixed solvent becomes poorer for 5CB. As shown in Fig. 7, even a small increase in J will lead to a large shift in the phase diagram. When we use $J_A/T_{IN}^0 = 1.06$, $J_B/T_{IN}^0 = 2.46$ and $J_{AB} = 0$, the black, red and blue curves correspond to $\Psi = 0$, 0.1 and 0.25, respectively.

3 Conclusions and outlook

Our detailed experimental and theoretical investigation of mixtures containing 5CB and ethanol, with and without a small amount of water added, underscores just how complex LC phase diagrams can be when more than one component is involved. Considering the enormous amounts of published reports utilising 5CB as mesogen, and the ubiquitous use of ethanol as organic solvent, it is surprising that the isotropic–isotropic phase separation has not previously been reported for this mixture combination. This is likely due to the low temperature range in which the phenomenon occurs for the binary mixture, requiring cooling to well below room temperature. Because the nematic phase eventually develops at yet lower temperature, the resulting phase diagram is richer than most studied systems exhibiting liquid–liquid phase separation *via* spinodal decomposition. This may stimulate future investigations, for instance focusing on the role of the elastic energy of nematic nuclei in delaying phase transitions.

The dramatic increase in temperature range of the isotropic–isotropic miscibility gap as a small amount of water is added is

remarkable. As only a slice of the ternary 5CB–ethanol–water phase diagram was presented here, there is much room for future studies providing a more complete picture. Our theoretical treatment provides a first attempt at explaining the sensitivity to the co-solvent as a result of the different affinity for the solute. We anticipate to find similar complexities occurring also for other solvent combinations. Possibly, a suitable way forward for handling the large parameter space when multiple solvents and mesogens are considered, may be to combine experimental data with predictive or machine learning algorithms to establish approximate phase diagrams for a variety of relevant LC–solvent compositions.

The discovery that water has such strong impact also has practical implications, since the phase separation with just 3 vol% water occurs at and even well above room temperature. Diluted ethanol or ethanol with a few percent of undeclared contaminants is commonly employed as solvent by experimentalists from various fields. Even if anhydrous solvents are utilised when preparing solutions, exposure to humid air will rapidly lead to water entering the solution, as a result of condensation due to ethanol evaporation-induced cooling.[28] Therefore, anomalies or difficulties encountered when attempting to mix polymer solutions or solvent mixtures with LCs may be the consequence of coexisting phases forming in solutions without researchers realising.

A particularly interesting case to further investigate is that of coaxial fibres with 5CB core produced by electrospinning from a single solution of 5CB, polymer and different types of alcohol solvents.[20,21] While the outcome has been explained as a result of *in situ* phase separation, the reason for this has not been fully elucidated. If the origin is the miscibility gap of 5CB and alcohol solvents, then this may explain why recent attempts to produce liquid crystal elastomer core–polymer sheath fibres using reactive mesogens with a chemical structure distinctly different from 5CB (the mesogen contained no cyano group) failed to produce a continuous core that could be separated from the supporting sheath.[44] There are thus good reasons to establish phase diagrams also of other mesogens in different solvents, possibly also with co-solvents present. The phase separation phenomenon does not require that the mesogen itself is mixed with the solvent, but it may occur due to contact with polymer solutions, for instance during coaxial electrospinning.[19,45,46]

Finally, another interesting challenge lies in identifying the ideal techniques for investigating these issues experimentally. While our study provides ample visible evidence of the various phase separation and phase transition phenomena, the frequent difficulties to reconcile transition temperatures with those detected in DSC investigations—in some cases with repeatability problems even in DSC—highlights the severe impact that spatial concentration gradients induced by the phase separation has on experiments. One approach to minimise these effects may be to strongly compartmentalise samples used for POM investigations or to include magnetic microparticles that can be used to mechanically stir the mixture within the test cell using an external magnetic field. We can conclude from our study that standard LC test cells with sample extensions on the order of centimetres otherwise do not allow homogenisation of the mixture even after days of annealing in case of prior phase separation. This situation should be considered for any experiments on LC mixtures in such test cells, as a first-order transition such as melting or clearing will lead to concentration gradients, which may or may not be significant depending on the phase diagram.

4 Experimental

Sample preparation procedures are described in detail in the ESI.†

4.1 Materials

5CB was acquired from two sources: Synthon Chemicals GmbH Co. and Yantai Xianhua Chem-Tech. Co. Ltd. The pure compound from both companies share a similar nematic to isotropic clearing point between 35.7 °C and 35.8 °C. Anhydrous ethanol was purchased from Merck KGaA ("ethanol for molecular biology", purity $\geq$99.8 vol% by GC, item #: 1.08543.0250). A 40 mL aliquot was stored under molecular sieves (size 4 Å, VWR Chemicals), which had been dried in an oven overnight at 70 °C before use. The aqueous ethanol mixture was based on this anhydrous ethanol, adding 4 mass% deionised water (conductivity: $\sim$0.055 μS).

4.2 POM investigation procedure

Mixtures were filled into square cross section glass capillaries (CM Scientific Ltd) for POM examination, one at a time. The capillaries were placed in a Linkam TMS120E temperature control stage with Peltier cooling, regulated by a Linkam T95PE controller. The stage was mounted onto an Olympus BX51 microscope equipped with a Canon EOS 760D digital camera for video capture (1920 × 1080 resolution, 25 frames per second). The samples were observed in transmission between crossed polarisers, with and without a first-order λ (530 nm) plate inserted, as well as without polarisers, using 4× to 20× objectives.

4.3 DSC measurements

Calorimetric measurements were performed with a DSC823e from Mettler-Toledo. The calibration of temperature and heat flow was done with indium and water. The masses of the samples examined by calorimetry ranged between 4 and 8 mg. Samples were filled into aluminum pans closed with a lid (volume: 40 μL; weight: about 50 mg). Tightness of crucibles was checked by weighing before and after the DSC measurements.

Conflicts of interest

There are no conflicts of interest to declare.

Acknowledgements

We are grateful to Dr C. Schütz for suggesting that we repeat our initial experiments conducted with lab-grade 96 vol%

ethanol (leading to our discovery of the coexisting isotropic phases at room temperature) using anhydrous ethanol, to assess the impact of water. We also thank O. Astasheva for help with the DSC experiments. Financial support from the European Research Council under the European Union's Seventh Framework Programme (FP/2007-2013)/ERC Grant Agreement no. 648763 (consolidator project INTERACT) is gratefully acknowledged. T. A. acknowledges the support from JSPS KAKENHI Grants no. JP17K05612, and JST CREST Grant no. JPMJCR1424, Japan.

References

1 P. S. Drzaic, *Liquid crystal dispersions*, World Scientific, Singapore, 1995.
2 K. R. Amundson and M. Srinivasarao, *Phys. Rev. E: Stat. Phys., Plasmas, Fluids, Relat. Interdiscip. Top.*, 1998, **58**, R1211.
3 J. W. Doane, N. A. Vaz, B.-G. Wu and S. Zumer, *Appl. Phys. Lett.*, 1986, **48**, 269–271.
4 P. S. Drzaic, *Liq. Cryst.*, 1988, **3**, 1543–1559.
5 Y. Lansac, F. Fried and P. Maïssa, *Liq. Cryst.*, 1995, **18**, 829–837.
6 H. Tanaka and T. Araki, *Chem. Eng. Sci.*, 2006, **61**, 2108–2141.
7 T. Araki and H. Tanaka, *Phys. Rev. Lett.*, 2004, **93**, 015702.
8 H. Nakazawa, S. Fujinami, M. Motoyama, T. Ohta, T. Araki and H. Tanaka, *Mol. Cryst. Liq. Cryst.*, 2001, **366**, 871–878.
9 H. Nakazawa, S. Fujinami, M. Motoyama, T. Ohta, T. Araki, H. Tanaka, T. Fujisawa, H. Nakada, M. Hayashi and M. Aizawa, *Comput. Theor. Polym. Sci.*, 2001, **11**, 445–458.
10 P. Palffy-muhoray, J. J. De Bruyn and D. A. Dunmur, *Mol. Cryst. Liq. Cryst.*, 1985, **127**, 301–319.
11 M. Urbanski, C. G. Reyes, J. Noh, A. Sharma, Y. Geng, V. S. R. Jampani and J. P. F. Lagerwall, *J. Phys.: Condens. Matter*, 2017, **29**, 133003.
12 J. Noh, V. S. R. Jampani, O. Haba, K. Yonetake, H. Takezoe and J. P. F. Lagerwall, *J. Mol. Liq.*, 2018, **267**, 197–204.
13 V. S. R. Jampani, D. J. Mulder, K. R. De Sousa, A.-H. Gélébart, J. P. F. Lagerwall and A. P. H. J. Schenning, *Adv. Funct. Mater.*, 2018, **28**, 1801209.
14 J.-G. Kim and S.-Y. Park, *Adv. Opt. Mater.*, 2017, **5**, 1700243.
15 S. Lee, H. Seo, Y. Kim and S. Kim, *Adv. Mater.*, 2017, **29**, 1606894.
16 J. Kang, S. Kim, A. Fernandez-Nieves and E. Reichmanis, *J. Am. Chem. Soc.*, 2017, **139**, 5708–5711.
17 J. D. Davies, D. R. Vaccaro, A. M. Morris, S. N. Herzer, A. P. H. J. Schenning and C. W. M. Bastiaansen, *Adv. Funct. Mater.*, 2013, **23**, 2723–2727.
18 C. L. van Oosten, C. W. M. Bastiaansen and D. J. Broer, *Nat. Mater.*, 2009, **8**, 677–682.
19 C. G. Reyes, A. Sharma and J. P. F. Lagerwall, *Liq. Cryst.*, 2016, **43**, 1986–2001.
20 E. A. Buyuktanir, M. W. Frey and J. L. West, *Polymer*, 2010, **51**, 4823–4830.
21 J. Wang, A. Jákli and J. West, *ChemPhysChem*, 2016, **17**, 3080–3085.
22 J. Wang, A. Jákli and J. West, *ChemPhysChem*, 2015, **16**, 1839–1841.
23 V. Anderson, E. M. Terentjev, S. P. Meeker, J. Crain and W. C. K. Poon, *Eur. Phys. J. E: Soft Matter Biol. Phys.*, 2001, **4**, 11–20.
24 T. Wood, J. Lintuvuori, A. Schofield, D. Marenduzzo and W. Poon, *Science*, 2011, **333**, 79–83.
25 Y. Kim, X. Wang, P. Mondkar, E. Bukusoglu and N. Abbott, *Nature*, 2018, **557**, 539–544.
26 L. Serrano, M. Fornerod, Y. Yang, S. Gaisford, F. Stellacci and S. Guldin, *Soft Matter*, 2018, **14**, 4615–4620.
27 P. Poulin, H. Stark, T. C. Lubensky and D. A. Weitz, *Science*, 1997, **275**, 1770–1773.
28 C. Law, T. Xiong and C. Wang, *Int. J. Heat Mass Transfer*, 1987, **30**, 1435–1443.
29 S. Yabunaka and T. Araki, *Phys. Rev. E: Stat., Nonlinear, Soft Matter Phys.*, 2011, **83**, 061711.
30 A. J. Liu and G. Fredrickson, *Macromolecules*, 1993, **26**, 2817.
31 C. Schen and T. Kyu, *J. Chem. Phys.*, 1995, **102**, 556.
32 M. Doi, T. Shimada and K. Okano, *J. Chem. Phys.*, 1988, **88**, 4070.
33 T. Araki and H. Tanaka, *J. Phys.: Condens. Matter*, 2006, **18**, L305.
34 J.-I. Fukuda, *Phys. Rev. E: Stat., Nonlinear, Soft Matter Phys.*, 1999, **59**, 3275.
35 A. Matsuyama, R. Evans and M. Cates, *Phys. Rev. E: Stat., Nonlinear, Soft Matter Phys.*, 2000, **61**, 2977.
36 A. Lapena, C. Gloctzer, S. Langer and A. J. Liu, *Phys. Rev. E: Stat., Nonlinear, Soft Matter Phys.*, 1999, **60**, R29.
37 P. Olmsted and P. Goldbart, *Phys. Rev. A: At., Mol., Opt. Phys.*, 1990, **41**, 4578.
38 A. Lacasta, J. Sancho and C. Yeung, *EPL*, 1994, **27**, 291.
39 E. D. Siggia, *Phys. Rev. A: At., Mol., Opt. Phys.*, 1979, **20**, 595.
40 A. Onuki, *Phase transition dynamics*, Cambridge University Press, 2002.
41 R. L. Scott, *J. Chem. Phys.*, 1948, **17**, 268.
42 J. A. Gonzalez-Leon and A. M. Mayes, *Macromolecules*, 2003, **36**, 2508–2515.
43 Y. Uematsu and T. Araki, *J. Chem. Phys.*, 2012, **137**, 024902.
44 A. Sharma and J. P. F. Lagerwall, *Materials*, 2018, **11**, 393.
45 J. Lin, C. Chen, L. Chen, Y. Chuang, S. Huang and C. Lee, *Opt. Express*, 2016, **24**, 3112–3126.
46 Y. Kye, C. Kim and J. Lagerwall, *J. Mater. Chem. C*, 2015, **3**, 8979–8985.

